

Data-Based and Opportunistic Integral Concurrent Learning for Adaptive Trajectory Tracking During Switched FES-Induced Biceps Curls

Brendon C. Allen^{ID}, *Member, IEEE*, Kimberly J. Stubbs^{ID}, *Graduate Student Member, IEEE*, and Warren E. Dixon^{ID}, *Fellow, IEEE*

Abstract—Hybrid exoskeletons, which combine functional electrical stimulation (FES) with a motorized testbed, can potentially improve the rehabilitation of people with movement disorders. However, hybrid exoskeletons have inherently nonlinear and uncertain dynamics, including combinations of discrete modes that switch between different continuous dynamic subsystems, which complicate closed-loop control. A particular complication is the uncertain muscle control effectiveness associated with FES. In this work, adaptive integral concurrent learning (ICL) motor and FES controllers are developed for a hybrid biceps curl exoskeleton, which are designed to achieve opportunistic and data-based learning of the uncertain human and electromechanical testbed parameters. Global exponential trajectory tracking and parameter estimation errors are proven through a Lyapunov-based stability analysis. The motor effectiveness is assumed to be unknown, and, to help with fatigue reduction, FES is enabled to switch between multiple electrodes on the biceps brachii, further complicating the analysis. A consequence of switching between the different uncertain subsystems is that the parameters must be opportunistically learned for each subsystem (i.e. each electrode and the motor), while that subsystem is active. Experiments were performed to validate the developed ICL controllers on twelve healthy participants. The average (\pm standard deviation) position tracking errors across each participant were 1.44 ± 5.32 deg, -0.25 ± 2.85 deg, and -0.17 ± 2.66 deg across biceps Curls 1-3, 4-7, and 8-10, respectively, where the average across the entire experiment was 0.28 ± 3.53 deg.

Manuscript received 7 September 2021; revised 28 March 2022, 18 July 2022, and 9 August 2022; accepted 23 August 2022. Date of publication 5 September 2022; date of current version 15 September 2022. This work was supported in part by the National Defense Science and Engineering Graduate Fellowship Program; in part by the Assistant Secretary of Defense for Health Affairs, through the Congressionally Directed Medical Research Program, under Award W81XWH1910330; and in part by the NSF under Award 1762829. (*Corresponding author: Brendon C. Allen.*)

This work involved human subjects or animals in its research. Approval of all ethical and experimental procedures and protocols was granted by the University of Florida Institutional Review Board under Application No. IRB201701089.

Brendon C. Allen is with the Department of Mechanical Engineering, Auburn University, Auburn, AL 36849 USA (e-mail: bca0027@auburn.edu).

Kimberly J. Stubbs and Warren E. Dixon are with the Department of Mechanical and Aerospace Engineering, University of Florida, Gainesville, FL 32611 USA (e-mail: kimberlystubbs@ufl.edu; wdixon@ufl.edu).

Digital Object Identifier 10.1109/TNSRE.2022.3204247

Index Terms—Functional electrical stimulation (FES), integral concurrent learning (ICL), parameter identification, switched systems, rehabilitation robotics, Lyapunov methods.

I. INTRODUCTION

A POTENTIAL rehabilitative exercise for people with upper limb movement disorders is functional electrical stimulation (FES) induced biceps curls [1], [2], [3], [4]. However, closed-loop FES control of muscle effort is challenging since the muscle effectiveness is unknown, the muscle dynamics are both nonlinear and uncertain, and high stimulation inputs are often uncomfortable [5], [6]. Furthermore, rehabilitative hybrid exoskeletons, which combine FES and motor control, must alternate control between FES and a motor without compromising performance.

Closed-loop FES control has previously been implemented on a range of rehabilitative exercises, such as rowing [7], cycling [8], [9], [10], [11], [12], walking [13], leg extensions [14], [15], [16], [17], and biceps curls [1], [2], [3], [4], among others. To compensate for system uncertainties, and to ensure stability, many closed-loop FES controllers have included only robust (i.e., high (infinite) frequency and/or high-gain) feedback terms (cf. [1], [2], [3], [16], [17]). An added motivation for such robust controllers is that they often produce a negative definite derivative of a strict Lyapunov function, which aids the stability analysis of a switched system (i.e., a system with mixed continuous and discrete dynamics, also called a hybrid system). However, the high-gain/high-frequency nature of robust FES control tends to increase the rate of fatigue and may also be uncomfortable for the participant [8]. Motivated to reduce the high-gain/high-frequency feedback terms, some results have augmented FES controllers with adaptive feedforward terms (cf. [7], [8], [9], [10], [11], [12], [13], [14], [15]) to ensure asymptotic trajectory tracking. The adaptive controllers in [7], [8], [9], [10], [11], and [14] implemented model-free techniques ranging from repetitive (RLC) and iterative (ILC) learning control, neural networks (NN), and fuzzy logic, whereas [12], [13], [15], [18], [19] implemented model-based techniques.

Although adaptive controllers are often used to improve control performance, sometimes it is desired for the adaptive

controller to simultaneously ensure parameter/system identification. Traditional adaptive controllers (cf. [20], [21]) can yield both exponential tracking and parameter identification provided the persistence of excitation (PE) condition is satisfied. However, the PE condition cannot be verified, in general, for nonlinear systems, and if the PE condition is unsatisfied there may be periods of oscillatory or unstable behavior (i.e., the bursting phenomenon [22]). In an effort to relax the PE condition and to enable online parameter/model identification, methods such as initial excitation (IE) [23], [24], concurrent learning (CL) [25], [26], [27], and integral concurrent learning (ICL) [28], [29] were recently developed. IE relaxes the PE condition by using low pass filters and a switched parameter estimator; whereas, CL and ICL require a more mild finite excitation (FE) condition. Both CL and ICL update the parameter estimates online using prior input/output data, which enables exponential tracking and parameter estimation. Furthermore, ICL eliminates the possibility of bursting errors and, unlike CL, does not require the highest order derivative to be known [28].

To date, ICL was previously implemented on a FES system in the authors' preliminary work [19], which this work is built upon, and in [18]; however, unlike in this work, [18] assumes the muscle effectiveness is known. ICL is motivated for a FES system since it may increase the FES controller's efficiency and potentially yield smaller FES inputs (e.g., the high-gain/high-frequency robust terms can be reduced), which ultimately may reduce fatigue and increase the participant's comfort [8]. Furthermore, ICL yields exponential tracking and parameter identification, which allows for the human and machine dynamics to be learned online.

Building upon our work in [19], adaptive ICL motor and FES controllers were developed for an uncertain nonlinear hybrid biceps curl exoskeleton. Additionally, a complete switched systems Lyapunov-like stability analysis was performed to ensure global exponentially decaying parameter estimation and trajectory tracking errors. Similar to [19], FES is applied during desired elbow flexion, and the motor is applied during desired elbow extension. Unlike our work in [19], this paper assumes the motor effectiveness is unknown, allows for FES control to switch between multiple electrodes, and provides comparative experiments on twelve healthy participants to validate the control development. Allowing FES to switch control between multiple electrodes on the biceps brachii allows for fatigue to be further reduced [2]; however, it also complicates the analysis and required the model, control development, and stability analysis to be greatly modified compared to our work in [19]. This work is differentiated from prior ICL developments, such as those in [19], [28], and [18], since this work involves switching between multiple control inputs that each have an uncertain (and potentially different) control effectiveness, which results in different uncertain parameters for each control subsystem. The solution is to perform opportunistic learning by updating the parameters and recording input/output data for each subsystem, while that subsystem is active. After sufficient learning has occurred for a given subsystem, its parameters are able to be updated regardless of the currently active subsystem. Comparative experiments were performed on twelve healthy participants using the developed

control system, a traditional adaptive controller, and a robust controller resulting in average (\pm standard deviation) position tracking errors of 0.28 ± 3.53 deg, 1.47 ± 5.78 deg, and 3.36 ± 7.97 deg, respectively, across a 10 curl experiment. The results indicated improved tracking performance for the ICL controller compared to some traditional adaptive and robust controllers, while providing similar average FES and motor control inputs. The results further demonstrated the ability of the ICL controller to improve the tracking performance as adaptation occurred. Efforts to perform preliminary experiments on participants with neurological conditions were stymied due to Covid-19.

II. DYNAMICS

The dynamics of the uncertain nonlinear hybrid biceps curl exoskeleton are modeled as¹ [2]

$$M(\ddot{q}) + G(q) + P(q, \dot{q}) + B_d(\dot{q}) = \tau_e(t) + \tau_M(t), \quad (1)$$

where $q : \mathbb{R}_{\geq 0} \rightarrow \mathcal{Q}$, $\dot{q} : \mathbb{R}_{\geq 0} \rightarrow \mathbb{R}$, and $\ddot{q} : \mathbb{R}_{\geq 0} \rightarrow \mathbb{R}$ denote the measured angle, measured angular velocity, and unmeasurable acceleration, respectively, of the forearm about the elbow joint. The set $\mathcal{Q} \subset \mathbb{R}$ denotes a compact set of potential forearm angles. The inertial, gravitational, passive viscoelastic tissue, and damping effects of the hybrid biceps curl exoskeleton are denoted by $M : \mathbb{R} \rightarrow \mathbb{R}_{>0}$, $G : \mathcal{Q} \rightarrow \mathbb{R}$, $P : \mathcal{Q} \times \mathbb{R} \rightarrow \mathbb{R}$, and $B_d : \mathbb{R} \rightarrow \mathbb{R}$, respectively, and are defined as

$$M(\ddot{q}) \triangleq J\ddot{q}, \quad G(q) \triangleq mgl \cos(q - \theta_0), \quad (2)$$

$$P(q, \dot{q}) \triangleq k_{e1}(q - k_{e2}) + b_v\dot{q}, \quad B_d(\dot{q}) \triangleq b_d\dot{q}, \quad (3)$$

where $J, m, g, l, b_v, b_d \in \mathbb{R}_{>0}$ and $k_{e1}, k_{e2} \in \mathbb{R}$ are unknown constants and $\theta_0 \in \mathbb{R}_{>0}$ is a known constant.

In this paper, FES is applied via multiple electrodes that are placed on the biceps brachii muscle using $w \in \mathbb{N}$ distinct channels of a stimulator, where $m \in \mathcal{M} \triangleq \{1, 2, \dots, w\}$ indicates the m^{th} electrode channel, and \mathcal{M} is a finite set. The torques produced about the elbow joint due to the motor and FES-induced muscle contractions are denoted by $\tau_e, \tau_M : \mathbb{R}_{\geq 0} \rightarrow \mathbb{R}$, respectively, and defined as

$$\tau_e(t) \triangleq b_e U_e(t), \quad \tau_M(t) \triangleq \sum_{m \in \mathcal{M}} b_m U_m(t), \quad (4)$$

where $b_e, b_m \in \mathbb{R}_{>0}$ denote the unknown and constant control effectiveness terms for the motor and stimulation via the m^{th} electrode over the biceps brachii muscle,² respectively. The current input to the motor and the stimulation (i.e., pulse width) input for each electrode are denoted by $U_e : \mathbb{R}_{\geq 0} \rightarrow \mathbb{R}$ and $U_m : \mathbb{R}_{\geq 0} \rightarrow \mathbb{R}, \forall m \in \mathcal{M}$, respectively, and defined as

$$U_e(t) \triangleq K_e \sigma_e(\dot{q}_d) u_e(t), \quad U_m(t) \triangleq K_m \sigma_m(q, \dot{q}_d) u_m(t), \quad (5)$$

¹For notational brevity, all explicit dependence on time, t , within the terms $q(t)$, $\dot{q}(t)$, and $\ddot{q}(t)$ is suppressed.

²Due to unknown effects associated with changing muscle geometry, the control effectiveness of stimulation varies with the angle of the elbow. However, if each electrode is placed properly then the biceps can be split into distinct stimulation regions for each electrode, where the control effectiveness is approximately constant over each electrode's stimulation region [2], [4]. An open problem for future work that may yield improved performance is to consider the position and velocity dependency of the muscles along with a stability analysis that accounts for such effects.

$\forall m \in \mathcal{M}$, where $u_e, u_m : \mathbb{R}_{\geq 0} \rightarrow \mathbb{R}$ represent the subsequently designed motor and FES control inputs, respectively, $K_e, K_m \in \mathbb{R}_{>0}$ represent selectable constants, and $q_d, \dot{q}_d, \ddot{q}_d : \mathbb{R}_{\geq 0} \rightarrow \mathbb{R}$ represent the bounded desired position, velocity, and acceleration, respectively. The motor switching signal, $\sigma_e : \mathbb{R} \rightarrow \{0, 1\}$, and the FES switching signal for the m^{th} electrode, $\sigma_m : \mathcal{Q} \times \mathbb{R} \rightarrow \{0, 1\}$, are respectively defined as

$$\sigma_e(\dot{q}_d) \triangleq \begin{cases} 1, & \dot{q}_d < 0 \\ 0, & \text{otherwise} \end{cases}, \quad (6)$$

$$\sigma_m(q, \dot{q}_d) \triangleq \begin{cases} 1, & \dot{q}_d \geq 0 \text{ and } q \in \mathcal{Q}_m \\ 0, & \text{otherwise} \end{cases}, \quad \forall m \in \mathcal{M}, \quad (7)$$

where $\mathcal{Q}_m \subseteq \mathcal{Q}$ denotes the set of angles over which the m^{th} electrode channel is stimulated. In this paper, \mathcal{Q}_m is selected as in [4] and [2] such that \mathcal{Q}_m segments \mathcal{Q} and a single electrode is active at a time, that is $\bigcup_{m \in \mathcal{M}} \mathcal{Q}_m = \mathcal{Q}$ and $\bigcap_{m \in \mathcal{M}} \mathcal{Q}_m = \emptyset$. Furthermore, the switching signals in (6) and (7) are designed to apply the motor and FES only during desired elbow extension and flexion, respectively.³

Substituting (2), (4), and (5) into (1) yields⁴

$$\sum_{m \in \mathcal{M}} b_m K_m \sigma_m u_m + b_e K_e \sigma_e u_e = J\ddot{q} + G + P + B_d, \quad (8)$$

which can be rewritten as

$$\sum_{i \in \mathcal{S}} B_i \sigma_i u_i = J\ddot{q} + G + P + B_d, \quad (9)$$

where $B_i \triangleq b_i K_i$, and $i \in \mathcal{S} \triangleq \mathcal{M} \cup \{e\} = \{1, 2, \dots, w, e\}$ indicates the subsystem, which is either an electrode or the motor. By design of the switching signals in (6) and (7), whenever $\sigma_i = 1$ for any $i \in \mathcal{S}$, $\sigma_j = 0, \forall j \in \mathcal{S}, j \neq i$. The switched hybrid biceps curl exoskeleton system in (9) has the subsequent properties [2].

Property 1: The inertial effects are bounded such that $c_j \leq J \leq c_J$, where $c_j, c_J \in \mathbb{R}_{>0}$ are known constants.

Property 2: The control effectiveness, b_i , is bounded $\forall i \in \mathcal{S}$ such that $\underline{c}_i \leq B_i \leq \bar{c}_i$, where $\underline{c}_i, \bar{c}_i \in \mathbb{R}_{>0}$ are known constants.

Property 3: The switched system in (9) is linear in the unknown constant parameters. For example, when the i^{th} subsystem is active (i.e., $\sigma_i = 1$ and $\sigma_j = 0, \forall j \in \mathcal{S}, j \neq i$) the following definition holds:

$$Y_1 \theta_i \triangleq \frac{1}{B_i} (J\ddot{q} + G + P + B_d), \quad (10)$$

where $Y_1 \in \mathbb{R}^{1 \times p}$ denotes a known regression matrix, $\theta_i \in \mathbb{R}^p$ denotes the unknown constant parameters for the i^{th} subsystem, and p denotes the number of uncertain parameters.

³FES-induced muscle activation can only produce a positive torque and negative FES inputs are set to zero during implementation. Therefore, the switching signals in (6) and (7) could result in uncontrolled regions; however, this situation was not observed during the subsequent experimental analysis. If desired, the switching signals in (6) and (7) could be modified to set $\sigma_m = 0$ if $u_m \leq 0$ and to set $\sigma_e = 1$ if $\sigma_m = 0, \forall m \in \mathcal{M}$.

⁴For notational brevity, all functional dependencies are hereafter suppressed unless required for clarity of exposition.

III. CONTROL DEVELOPMENT

A. Tracking Error Development

The objective of this paper is for the forearm to track a desired position and velocity. The position tracking error, $e_1 : \mathbb{R}_{\geq 0} \rightarrow \mathbb{R}$, is measurable and is defined as

$$e_1 \triangleq q_d - q. \quad (11)$$

An auxiliary tracking error, $e_2 : \mathbb{R}_{\geq 0} \rightarrow \mathbb{R}$, is measurable and is defined as

$$e_2 \triangleq \dot{e}_1 + \alpha e_1, \quad (12)$$

where $\alpha \in \mathbb{R}_{>0}$ is a selectable constant. To obtain the open-loop error system for the i^{th} subsystem (i.e., when $\sigma_i = 1$), we take the derivative of (12), multiply both sides by J , and use (9) to yield

$$J\dot{e}_2 = B_i (Y_2 \theta_i - u_i), \quad \sigma_i = 1, \quad (13)$$

for any $i \in \mathcal{S}$, where $Y_2 \in \mathbb{R}^{1 \times p}$ denotes a measurable matrix, θ_i is defined in (10), and $Y_2 \theta_i$ is defined as

$$Y_2 \theta_i \triangleq \frac{1}{B_i} (J\ddot{q}_d + G + P + B_d + \alpha J \dot{e}_1). \quad (14)$$

B. Parameter Identification Development

The parameter identification error vector for the i^{th} subsystem, $\tilde{\theta}_i \in \mathbb{R}^p$, is defined $\forall i \in \mathcal{S}$ as

$$\tilde{\theta}_i \triangleq \theta_i - \hat{\theta}_i, \quad (15)$$

where $\hat{\theta}_i \in \mathbb{R}^p$ denotes the parameter estimates for the i^{th} subsystem. Based on the subsequent stability analysis, an update law for the i^{th} subsystem's parameter estimates is designed $\forall i \in \mathcal{S}$ as

$$\dot{\hat{\theta}}_i \triangleq \begin{cases} \Gamma_i Y_2^T e_2 + \gamma_i \Gamma_i S_i, & \sigma_i = 1 \\ 0, & \sigma_i = 0 \text{ and } \sigma_{i,l} = 0, \\ \gamma_i \Gamma_i S_i, & \sigma_i = 0 \text{ and } \sigma_{i,l} = 1 \end{cases}, \quad (16)$$

where $\Gamma_i \in \mathbb{R}^{p \times p}$ is a user-selectable diagonal and positive definite matrix, $\gamma_i \in \mathbb{R}_{>0}$ is a selectable constant, and S_i contains a history stack of previous ICL terms, and is defined $\forall i \in \mathcal{S}$ as

$$S_i \triangleq \sum_{j=1}^{N_i} \mathcal{Y}_{i,j}^T (\mathcal{U}_{i,j} - \mathcal{Y}_{i,j} \hat{\theta}_i), \quad (17)$$

where $N_i \in \mathbb{N}$ denotes the size of the history stack for the i^{th} subsystem. The switching signal, $\sigma_{i,l} : \mathbb{R}_{\geq 0} \rightarrow \{0, 1\}$, is designed to indicate when sufficient learning has been achieved for the i^{th} subsystem, and is defined $\forall i \in \mathcal{S}$ as

$$\sigma_{i,l}(t) \triangleq \begin{cases} 1 & \lambda_{\min} \left\{ \sum_{j=1}^{N_i} \mathcal{Y}_{i,j}^T \mathcal{Y}_{i,j} \right\} \geq \lambda_i \\ 0 & \lambda_{\min} \left\{ \sum_{j=1}^{N_i} \mathcal{Y}_{i,j}^T \mathcal{Y}_{i,j} \right\} < \lambda_i \end{cases}, \quad (18)$$

where $\lambda_i \in \mathbb{R}_{>0}, \forall i \in \mathcal{S}$ are selectable constants, and the minimum or maximum eigenvalue of $\{\cdot\}$ is indicated by

$\lambda_{\min}\{\cdot\}$ or $\lambda_{\max}\{\cdot\}$, respectively. To implement the ICL portion of the update laws, the following ICL terms are defined

$$\mathcal{Y}_i(t) \triangleq \begin{cases} 0_{1 \times p} & \sigma_i = 0 \\ 0_{1 \times p} & t - t_{n,on}^i \in [0, \Delta t], \\ \int_{t-\Delta t}^t Y_1(\kappa) d\kappa & t - t_{n,on}^i > \Delta t \end{cases}, \quad (19)$$

$$\mathcal{U}_i(t) \triangleq \begin{cases} 0 & \sigma_i = 0 \\ 0 & t - t_{n,on}^i \in [0, \Delta t], \\ \int_{t-\Delta t}^t \sigma_i u_i(\kappa) d\kappa & t - t_{n,on}^i > \Delta t \end{cases}, \quad (20)$$

$\forall i \in \mathcal{S}$, where $\Delta t \in \mathbb{R}_{>0}$ is a user-selectable constant that sets the size of the integration window, and $0_{1 \times p}$ denotes a $1 \times p$ matrix of zeros. For the i^{th} subsystem, let the n^{th} time instant when σ_i becomes nonzero be denoted by $t_{n,on}^i$, and let the n^{th} time when σ_i becomes zero be denoted by $t_{n,off}^i$, where $i \in \mathcal{S}$, $n \in \{1, 2, \dots\}$. Notice from the definitions in (17), (19), and (20) that the history stacks of S_i contain previous input and output data. To select meaningful data for the history stack (i.e., not zeros), define $\mathcal{Y}_{i,j} \triangleq \mathcal{Y}_i(t_{i,j})$ and $\mathcal{U}_{i,j} \triangleq \mathcal{U}_i(t_{i,j})$ for the i^{th} subsystem, where $t_{i,j} \leq t$ is selected such that $t_{i,j} \in (t_{n,on}^i + \Delta t, t_{n,off}^i)$, $\forall n \in \{1, 2, \dots\}$. For the i^{th} subsystem (i.e., $\sigma_i = 1$), it can be shown that

$$\mathcal{Y}_{i,j} \theta_i = \mathcal{U}_{i,j}, \quad \forall t_{i,j} \in (t_{n,on}^i + \Delta t, t_{n,off}^i), \forall n, \quad (21)$$

by substituting (10) into (9), integrating both sides, and then using the definitions in (19) and (20). Now a non-implementable form of S_i can be obtained, to facilitate the subsequent stability analysis, by substituting (21) into (17) and using (15) to yield

$$S_i = \sum_{j=1}^{N_i} \mathcal{Y}_{i,j}^T \mathcal{Y}_{i,j} \tilde{\theta}_i. \quad (22)$$

Notice that the acceleration measurements are included in (10). However, an advantage of ICL compared to CL is that the ICL terms (19)-(20) are designed in such a way that acceleration is not required. The term $\int_{t-\Delta t}^t Y_1(\kappa) d\kappa$ from (19) is obtained for the i^{th} subsystem by integrating both sides of (10) to yield

$$\int_{t-\Delta t}^t Y_1(\kappa) \theta_i d\kappa \triangleq Y_3 \theta_i + \int_{t-\Delta t}^t Y_4(\kappa) \theta_i d\kappa, \quad (23)$$

$\forall t \in (t_{n,on}^i + \Delta t, t_{n,off}^i)$, $\forall n$, where

$$Y_3 \theta_i \triangleq \frac{J}{B_i} (\dot{q}(t) - \dot{q}(t - \Delta t)), \quad (24)$$

$$Y_4 \theta_i \triangleq \frac{1}{B_i} (G + P + B_d). \quad (25)$$

Thus, (19) can be calculated without measuring the acceleration due to the design of (24), and (25).

C. Closed-Loop Error System

Based on the subsequent stability analysis, an adaptive controller is designed for each subsystem as

$$u_i = Y_2 \hat{\theta}_i + k_i e_2, \quad (26)$$

$\forall i \in \mathcal{S}$, where $k_i \in \mathbb{R}_{>0}$, $\forall i \in \mathcal{S}$ are selectable constants. The closed-loop error system for the i^{th} subsystem is obtained by substituting (26) into (13) to yield

$$J \dot{e}_2 = B_i (Y_2 \tilde{\theta}_i - k_i e_2), \quad \sigma_i = 1, \quad (27)$$

for any $i \in \mathcal{S}$.

IV. STABILITY ANALYSIS

A special characteristic of the update laws for the parameter estimates of each subsystem, as defined in (16), is that the typical PE criteria can be relaxed to yield a FE criteria for parameter estimation convergence, which is stated in Assumption 1.

Assumption 1: Sufficient excitation for the i^{th} subsystem occurs over a finite duration of time. Thus, $\exists T_i \in \mathbb{R}_{>0}$, $\forall i \in \mathcal{S}$ such that $\forall t \geq T_i$ learning is complete for the i^{th} subsystem (i.e., $\sigma_{i,l} = 1$), or in other words the following FE condition is satisfied: $\lambda_{\min} \left\{ \sum_{j=1}^{N_i} \mathcal{Y}_{i,j}^T \mathcal{Y}_{i,j} \right\} \geq \lambda_i$, $\forall t \geq T_i$. Learning across all subsystems is considered complete for $\forall t \geq T$, where $T \in \mathbb{R}_{>0} \triangleq \max \{T_i \mid i \in \mathcal{S}\}$.⁵

To facilitate the subsequent analysis, we define a common Lyapunov function candidate, $V : \mathbb{R}^{2+p(w+1)} \rightarrow \mathbb{R}_{\geq 0}$, that is both continuously differentiable and positive define as

$$V \triangleq \frac{1}{2} e_1^2 + \frac{1}{2} J e_2^2 + \sum_{i \in \mathcal{S}} \frac{1}{2} B_i \tilde{\theta}_i^T \Gamma_i^{-1} \tilde{\theta}_i. \quad (28)$$

Notice that (28) can be bounded as

$$\underline{\lambda} \|z\|^2 \leq V \leq \bar{\lambda} \|z\|^2, \quad (29)$$

where $\underline{\lambda}, \bar{\lambda} \in \mathbb{R}_{>0}$ are known constants defined as

$$\underline{\lambda} \triangleq \frac{1}{2} \min \left\{ 1, c_j, \underline{c}_i \lambda_{\min} \left\{ \Gamma_i^{-1} \right\} \mid i \in \mathcal{S} \right\},$$

$$\bar{\lambda} \triangleq \frac{1}{2} \max \left\{ 1, c_J, \bar{c}_i \lambda_{\max} \left\{ \Gamma_i^{-1} \right\} \mid i \in \mathcal{S} \right\},$$

and $z \in \mathbb{R}^{2+p(w+1)}$ is defined as

$$z \triangleq [e_1 \ e_2 \ \tilde{\theta}_1^T \ \tilde{\theta}_2^T \ \dots \ \tilde{\theta}_w^T \ \tilde{\theta}_e^T]^T. \quad (30)$$

Theorem 1: For the dynamic system in (9) with Properties 1-3, the controllers defined in (26) and the adaptive update laws defined in (16) ensure global bounded parameter estimation and trajectory tracking errors for $t \in [0, T)$, provided the following sufficient conditions are met⁶

$$\alpha > \frac{1}{2}, \quad k_i > \frac{1}{2\underline{c}_i}, \quad \forall i \in \mathcal{S}. \quad (31)$$

Proof: Since the update laws in (16) and the closed-loop error system in (27) are discontinuous, the solution to the time derivative of (28) exists almost everywhere (a.e.) within $t \in [t_0, \infty)$. There exists a generalized time derivative

⁵The FE condition requires the system to be sufficiently excited, and unlike the PE condition, can be verified online during run-time execution. Increasing the number of data points in the history stack helps to satisfy the FE condition.

⁶The results in Theorem 1 hold even if Assumption 1 is never satisfied; however, in this case $T = \infty$. When Assumption 1 is satisfied, the subsequently developed Theorem 2 can be used to prove additional results.

of V , denoted by \dot{V} , where $\dot{V}(z) \stackrel{\text{a.e.}}{\in} \dot{V}(z)$. Let $z(t)$ for $t \in [t_0, \infty)$ be a Filippov solution to the differential inclusion $\dot{z} \in K[h](z)$, where $K[\cdot]$ is defined as in [30], and $h \triangleq \begin{bmatrix} \dot{e}_1 & \dot{e}_2 & \dot{\theta}_1 & \dot{\theta}_2 & \dots & \dot{\theta}_w & \dot{\theta}_e \end{bmatrix}^T$ [31]. Taking the time derivative of (28) and substituting in (12) yields

$$\begin{aligned} \dot{V} \subseteq & e_1(e_2 - ae_1) + e_2K[J\dot{e}_2] \\ & - \sum_{i \in \mathcal{S}} B_i \tilde{\theta}_i^T \Gamma_i^{-1} K[\dot{\theta}_i]. \end{aligned} \quad (32)$$

Consider the case when $\sigma_i = 1$ for some $i \in \mathcal{S}$ such that $\dot{\theta}_i, \forall i \in \mathcal{S}$ and $J\dot{e}_2$ are continuous according to (16) and (27). Substituting (16) and (22) for the i^{th} subsystem into (32), substituting (27) into (32), using the fact that $\dot{V}(z) \stackrel{\text{a.e.}}{\in} \dot{V}(z)$, and canceling common terms yields

$$\begin{aligned} \dot{V} \stackrel{\text{a.e.}}{\in} & -ae_1^2 - B_ik_ie_2^2 - \gamma_i B_i \tilde{\theta}_i^T \sum_{j=1}^{N_i} \mathcal{Y}_{i,j}^T \mathcal{Y}_{i,j} \tilde{\theta}_i \\ & - \sum_{\substack{k \in \mathcal{S} \\ k \neq i}} B_k \tilde{\theta}_k^T \Gamma_k^{-1} \dot{\theta}_k + e_1 e_2, \end{aligned} \quad (33)$$

for the case when $\sigma_i = 1$. When $\sigma_i = 1$, (16) and (22) can be used to determine that for a given $k \in \mathcal{S}$, $\dot{\theta}_k = 0$ (when $\sigma_{k,l} = 0$) or $\dot{\theta}_k = \gamma_k \Gamma_k \sum_{j=1}^{N_k} \mathcal{Y}_{k,j}^T \mathcal{Y}_{k,j} \tilde{\theta}_k$ (when $\sigma_{k,l} = 1$). Since time is restricted to the time interval $t \in [0, T)$, it is clear that learning is not yet complete for every subsystem according to Assumption 1. Therefore, it can conservatively be assumed that $\sum_{j=1}^{N_i} \mathcal{Y}_{i,j}^T \mathcal{Y}_{i,j}, \forall i \in \mathcal{S}$ is only positive semi-definite throughout the interval $t \in [0, T)$, and (33) can be upper bounded by using Young's Inequality and using Property 2 to yield

$$\dot{V} \stackrel{\text{a.e.}}{\leq} - \left(\alpha - \frac{1}{2} \right) e_1^2 - \left(k_i c_i - \frac{1}{2} \right) e_2^2, \quad (34)$$

$\forall t \in \left[t_{n,on}^i, t_{n,off}^i \right) \cap [0, T), \forall n$.

An overall upper bound for (34) can be determined across all subsystems as

$$\dot{V} \stackrel{\text{a.e.}}{\leq} - \left(\alpha - \frac{1}{2} \right) e_1^2 - \beta e_2^2, \quad (35)$$

$\forall t \in [0, T)$, where $\beta \triangleq \min \left\{ k_i c_i - \frac{1}{2} \mid i \in \mathcal{S} \right\}$.

By inspection of (28) and (35) it can be seen that $V \geq 0$ and $\dot{V} \leq 0, \forall t \in [0, T)$. Thus, from (28) it can be shown that $e_1, e_2, \theta_i \in \mathcal{L}_\infty, \forall i \in \mathcal{S}$ and from (15) it is clear that $\dot{\theta}_i \in \mathcal{L}_\infty, \forall i \in \mathcal{S}$. From (11), (12), and (14) it can be determined that $\dot{e}_1, q, \dot{q}, Y_2 \in \mathcal{L}_\infty$. Since $Y_2, \dot{\theta}_i, e_2 \in \mathcal{L}_\infty$ it can be seen that $u_i \in \mathcal{L}_\infty, \forall i \in \mathcal{S}$. By using (29) it can proven that

$$\|z(T)\| \leq \sqrt{\frac{\bar{\lambda}}{\underline{\lambda}}} \|z(0)\|. \quad (36)$$

■

global exponential parameter estimation and trajectory tracking errors for $t \in [0, \infty)$ in the sense that

$$\|z(t)\| \leq \frac{\bar{\lambda}}{\underline{\lambda}} \exp\left(\frac{\delta}{2\bar{\lambda}} T\right) \|z(0)\| \exp\left(-\frac{\delta}{2\bar{\lambda}} t\right), \quad (37)$$

where

$$\delta \triangleq \min \left\{ \alpha - \frac{1}{2}, c_i k_i - \frac{1}{2}, k_3 \lambda_e, \gamma_i \lambda_i c_i \mid i \in \mathcal{S} \right\}, \quad (38)$$

provided the conditions in (31) are satisfied.

Proof: First, consider the time interval $t \in [T, \infty)$. Notice that $\lambda_{\min} \left\{ \sum_{j=1}^{N_i} \mathcal{Y}_{i,j}^T \mathcal{Y}_{i,j} \right\} \geq \lambda_i, \forall i \in \mathcal{S}$ (i.e., $\sigma_{i,l} = 1, \forall i \in \mathcal{S}$) by Assumption 1, and hence, $\sum_{j=1}^{N_i} \mathcal{Y}_{i,j}^T \mathcal{Y}_{i,j}, \forall i \in \mathcal{S}$ is positive definite over the time interval $t \in [T, \infty)$. For the case when $\sigma_i = 1$, for some $i \in \mathcal{S}$, (33) can be rewritten by using (16) and the fact that $\sigma_{i,l} = 1, \forall i \in \mathcal{S}$ as

$$\dot{V} \stackrel{\text{a.e.}}{\in} e_1 e_2 - ae_1^2 - B_ik_ie_2^2 - \sum_{i \in \mathcal{S}} \gamma_i B_i \tilde{\theta}_i^T \sum_{j=1}^{N_i} \mathcal{Y}_{i,j}^T \mathcal{Y}_{i,j} \tilde{\theta}_i, \quad (39)$$

which can be upper bounded by using Young's Inequality, Assumption 1, and Property 2 to yield

$$\begin{aligned} \dot{V} \stackrel{\text{a.e.}}{\leq} & - \left(\alpha - \frac{1}{2} \right) e_1^2 - \left(c_i k_i - \frac{1}{2} \right) e_2^2 \\ & - \sum_{i \in \mathcal{S}} \gamma_i \lambda_i c_i \tilde{\theta}_i^T \tilde{\theta}_i, \end{aligned} \quad (40)$$

$\forall t \in \left[t_{n,on}^i, t_{n,off}^i \right) \cap [T, \infty), \forall n$. Using (29) and (38), where δ represents the most conservative decay rate for every subsystem (i.e., every $i \in \mathcal{S}$), an overall upper bound for (40) can be obtained as

$$\dot{V} \stackrel{\text{a.e.}}{\leq} -\frac{\delta}{\bar{\lambda}} V, \quad (41)$$

$\forall t \in [T, \infty)$, which verifies that (28) is a common Lyapunov function. The differential inequality in (41) can be solved and used with (29) to yield

$$\|z(t)\| \leq \sqrt{\frac{\bar{\lambda}}{\underline{\lambda}}} \|z(T)\| \exp\left(-\frac{\delta}{2\bar{\lambda}}(t-T)\right), \forall t \in [T, \infty). \quad (42)$$

An exponential bound can be obtained for all $t \in [0, \infty)$ by substituting (36) into (42) to yield the result in (37). From (30) and (42) it can be seen that $e_1, e_2, \tilde{\theta}_i \in \mathcal{L}_\infty, \forall i \in \mathcal{S}$, and a similar development from Theorem 1 can be used to show that $u_i \in \mathcal{L}_\infty, \forall i \in \mathcal{S}$ and the remaining signals are bounded. ■

V. EXPERIMENTS

The adaptive update law in (16) contains both ICL terms ($\gamma_i \Gamma_i S_i$) and more traditional adaptive terms ($\Gamma_i Y_2^T e_2$). Note that the ICL terms could be removed by setting $\gamma_i = 0, \forall i$ and all adaptive terms could be removed by setting Γ_i as a matrix of zeros $\forall i$. Hereafter, the developed control system in this work (i.e., (16) and (26)) is referred to as Controller A, the developed adaptive controller without ICL terms ($\gamma_i = 0, \forall i$) is referred to as Controller B (i.e., a traditional adaptive

Theorem 2: For the dynamic system in (9) with Properties 1-3, provided that Assumption 1 holds, the controllers defined in (26) and the adaptive update laws defined in (16) ensure

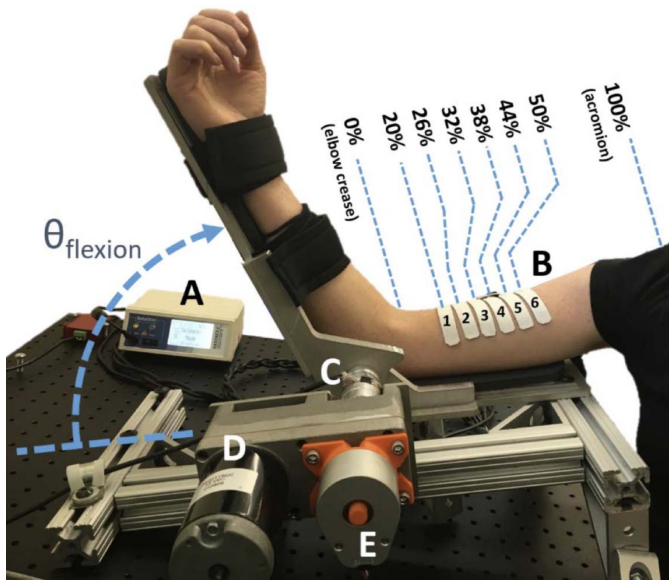


Fig. 1. The testbed consists of A) a stimulator, B) electrodes placed over the biceps, C) a torque sensor (not used), D) a gear motor, E) an encoder. The six electrode positions, labeled 1 through 6, are defined according to the above labeled percentages between the elbow crease and acromion. The depicted angle $\theta_{flexion}$ denotes the elbow angle, q . Note, the testbed has mechanical stops to prevent elbow hyperextension or hyperflexion. Figure is replicated from [4].

controller, cf. [20], [21]), and the developed controller with no adaptive terms (Γ_i as a matrix of zeros $\forall i$) is referred to as Controller C (i.e., a robust controller). For all three controllers, $\hat{\theta}(t_0) = [0, 0, 0, 0, 0]^T$. Comparative experiments using Controllers A, B, and C were performed to determine the effect of each of the adaptive terms on the system performance.

A. Experimental Testbed and Setup

The custom arm curl testbed detailed in [4] and [2] and depicted in Fig. 1 was used as the experimental testbed. The optical digital encoder, 27 Watt, parallel-shaft, brushed gear-motor, and Hasomed Rehaslim stimulator were interfaced in real-time at 1000 Hz using a desktop computer, MATLAB/Simulink, and a Quanser Q-PIDe DAQ board. The stimulator was used to input rectangular, symmetric, and biphasic pulses to the biceps at a fixed amplitude and frequency of 30 mA and 35 Hz, respectively, whereas the pulse width (PW) was set by the FES controller [3].

Prior to an experiment, the participant was seated in front of the testbed, their upper arm placed upon a stationary plate, and their forearm attached to a rotating plate as depicted in Fig. 1. Three electrodes (0.6" x 2.75"), labeled Electrodes 1, 2, and 3, were then respectively placed on the biceps brachii at positions 2, 4, and 5 according to Fig. 1, and a 3" times 5" electrode was placed on the shoulder to act as a reference for the smaller electrodes. The stimulation regions for Electrodes 1, 2, and 3 were defined (in deg) as $Q_1 \in [20, 45)$, $Q_2 \in (45, 70)$, $Q_3 \in (70, 100]$. These regions were sufficient to approximate the muscle control effectiveness as a constant, but additional regions or modeling parameter variation in the control effectiveness of the muscle, could yield improved

results.⁷ Prior to performing any experiment, saturation limits were obtained for each electrode to ensure comfort for the participant.

B. Experimental Protocol

Experiments were performed on six male and six female participants, aged 20-49 years old. Each participant provided written informed consent as approved by the University of Florida Institutional Review Board (IRB201701089).

During each experiment, the arm was initially fully extended (i.e., $q(t_0) = 0$ deg) and the desired angular position was defined as

$$q_d(t) \triangleq \begin{cases} \frac{\pi}{36}t & t \leq 5 \\ \frac{5\pi}{36} + \frac{7\pi}{36} \left(1 - \cos\left(\frac{t-5}{2}\right)\right) & t > 5 \end{cases}$$

The motor was used during the first 5 s to move forearm to 25 deg, after which the next 125.6 s consisted of either Controller A, B, or C being implemented to perform a total of 10 arm curls between 25 deg and 95 deg.

Experiments were performed using each participant's dominant arm, and Controllers A, B, and C were implemented in a random order. Participants were blind to the tracking performance during each experiment, and were asked to remain passive and provide no volitional effort. For each participant, a single experiment was performed using each controller.

As stated in Section III.B, data was recorded during the experiments to calculate (19) and (20) for each subsystem. Furthermore, to facilitate implementation a counter was developed and initialized at zero for each subsystem. For the i^{th} subsystem, whenever both (19) and (20) were non-zero, the counter for the i^{th} subsystem was increased by one and then the recorded values for (19) and (20) were included in the i^{th} subsystem's history stack in (17), until the history stack was full (i.e., the counter was at N_i). At this point, the counter was reset to zero. Subsequently, whenever both (19) and (20) were non-zero, they were added to the history stack if they increased the eigenvalue of the subsystem, otherwise the data was discarded. During the experiments, the following history stack parameters were implemented: $\lambda_i = 5 \times 10^{-6}$, $\forall i \in \mathcal{S}$, $N_i = 1000$, $\forall i \in \mathcal{S}$, and $\Delta t = 0.15$ s.

VI. RESULTS

Descriptive statistics of the position tracking error, motor effort, and FES effort are included in Table I. To demonstrate the effect of adaptation and to compare each controller, the results in Table I are averaged across each participant for Curls 1-3, 4-7, 8-10, and 1-10 (i.e., the overall results). Across each participant, the average (\pm standard deviation) position tracking errors were 1.44 ± 5.32 deg, 2.84 ± 7.40 deg, and 3.79 ± 8.14 deg across Curls 1-3 for Controllers A, B, and C, respectively, -0.25 ± 2.85 deg, 0.94 ± 5.31 deg, and 3.08 ± 7.85 deg across Curls 4-7 for Controllers A, B, and C, respectively, -0.17 ± 2.66 deg, 0.81 ± 4.78 deg, and

⁷From [2, Fig. 1], the torque produced from the electrodes at positions 2, 4, and 5 is approximately constant over the angle ranges (in deg) of 10 to 45, 45 to 70, and 70 to 100, respectively.

TABLE I
AVERAGE RESULTS FOR EACH CONTROLLER
ACROSS EACH PARTICIPANT

Control	Curls	RMS Error e_1 (deg)*	Peak Error e_1 (deg)†	Motor Effort (A)‡	FES Effort (μ s)¶
A	1-3	5.64	17.34	1.41±0.52	39.8±17.6
	4-7	3.00	10.27	1.43±0.50	39.5±14.7
	8-10	2.83	10.23	1.42±0.55	41.7±12.7
	1-10	3.74	17.98	1.42±0.52	40.2±15.0
B	1-3	8.30	23.53	1.41±0.56	42.8±20.0
	4-7	5.89	15.66	1.41±0.53	40.9±19.2
	8-10	5.50	14.53	1.40±0.54	43.1±19.1
	1-10	6.49	24.56	1.41±0.54	42.1±19.4
C	1-3	9.22	23.26	1.42±0.59	43.7±20.1
	4-7	9.11	22.41	1.44±0.56	40.8±19.2
	8-10	9.51	24.36	1.43±0.56	42.1±20.3
	1-10	9.26	27.36	1.43±0.57	42.0±19.8

* The root mean square (RMS) position error.

†The maximum absolute value of the position error.

‡The average \pm standard deviation (SD) of $|U_e|$ whenever U_e is nonzero, where U_e denotes the current input to the motor.

¶The average \pm SD of $\sum_{m \in \mathcal{M}} |U_m|$ whenever FES is applied, where U_m is the FES input into the m^{th} electrode.

3.32 ± 7.96 deg across Curls 8-10 for Controllers A, B, and C, respectively, and 0.28 ± 3.53 deg, 1.47 ± 5.78 deg, and 3.36 ± 7.97 deg across Curls 1-10 for Controllers A, B, and C, respectively. Typical position tracking, control input, and parameter estimate results for each controller are included in Figs. 2, 3, and 4, respectively, for a single participant. Note, the parameter estimates in Fig. 4 include the estimates for Electrodes 1-3 as a demonstration of typical estimation results for each subsystem. Furthermore, Controller C had no adaptation and was consequently not included in Fig. 4.

A. Statistical Analysis

Two sets of statistical tests were performed to investigate the effect of each controller and the effect of adaptation on the six measurements in Table I: the RMS position error, peak position error, and the mean and standard deviation (SD) of the motor effort and FES effort. In the first set of tests, Friedman tests were conducted to determine if the controller affected a given measurement across the entire experiment (i.e., Curls 1-10) and determined that the choice of controller had a significant effect on the median RMS position error (P-Value < 0.001), peak position error (P-Value = 0.014), and SD of the FES control effort (P-Value = 0.006). Due to the paired nature of the data (i.e., each controller was implemented on each participant), a series of two-sided paired Wilcoxon signed-rank tests with Bonferroni corrections on the P-Values were performed on the significant measurements from the Friedman tests and it was concluded that the median peak position error (P-Value = 0.505) and the median SD of the FES effort (P-Value = 1.0) were not significantly different for Controller B, compared to Controller C. Subsequently, one-sided paired Wilcoxon signed-rank tests with Bonferroni corrections were performed to conclude that Controller A, compared to Controller B, reduced the median RMS position error (P-Value = 0.001), median peak position error

(P-Value = 0.024), and median SD of the FES effort (P-Value = 0.002); Controller A, compared to Controller C, reduced the median RMS position error (P-Value = 0.001), median peak position error (P-Value = 0.024), and median SD of the FES effort (P-Value = 0.018); and Controller B, compared to Controller C, reduced the median RMS position error (P-Value = 0.013).

In the second set of tests, Friedman tests were conducted to determine, for each controller, if the curl groups (i.e., Curls 1-3, 4-7, and 8-10) affected each measurement and determined that the curl group had a significant effect on the median RMS position errors for Controllers A (P-Value < 0.001) and B (P-Value = 0.001), the median peak position errors for Controllers A (P-Value = 0.006) and B (P-Value = 0.039), and the median SD of the FES effort for Controller A (P-Value < 0.001). Two-sided paired Wilcoxon signed-rank tests with Bonferroni corrections were performed on the significant measurements from the second set of Friedman tests and it was concluded that there was no significant difference between Curl group 4-7, compared to Curl group 8-10, for the median RMS position error for Controllers A (P-Value = 0.904) and B (P-Value = 0.454), the median peak position error for Controllers A (P-Value = 1.0) and B (P-Value = 1.0), and the SD of the FES effort for Controller A (P-Value = 0.330). Likewise, one-sided paired Wilcoxon signed-rank tests with Bonferroni corrections were performed to conclude that Curl group 4-7, compared to Curl group 1-3, reduced the median RMS position error for Controllers A (P-Value = 0.001) and B (P-Value = 0.002), reduced the median peak position error for Controllers A (P-Value = 0.014) and B (P-Value = 0.018), and reduced the SD of the FES effort for Controller A (P-Value = 0.001); and Curl group 8-10, compared to Curl group 1-3, reduced the median RMS position error for Controllers A (P-Value = 0.001) and B (P-Value = 0.005), reduced the median peak position error for Controllers A (P-Value = 0.004) and B (P-Value = 0.014), and reduced the SD of the FES effort for Controller A (P-Value = 0.001).

VII. DISCUSSION

Using the data in Table I for Curls 1-10, Controller A, compared to Controller B (Controller C), decreased⁸ the RMS position error by 42.4% (59.6%), the peak position error by 26.8% (34.3%), the mean motor effort by -1.3% (0.5%), the SD of the motor effort by 4.2% (8.6%), the mean FES effort by 4.5% (4.3%), and the SD of the FES effort by 22.8% (24.2%). These results can be visually observed in Figs. 2 and 3 for a single participant. Furthermore, the statistical analysis confirmed that Controller A reduced the median position tracking error and the median SD of the FES effort relative to Controllers B and C and that Controller B improved the position tracking performance relative to Controller C. Therefore, it is clear that the adaptive controllers (Controllers A and B) outperformed a robust controller (Controller C) in position tracking; however, the addition of adaptive ICL terms (Controller A) further improved the position tracking performance

⁸Percent Decrease = $\frac{\text{Initial Value} - \text{Final Value (i.e., A value)}}{\text{Initial Value (i.e., B or C Value)}} \times 100$.

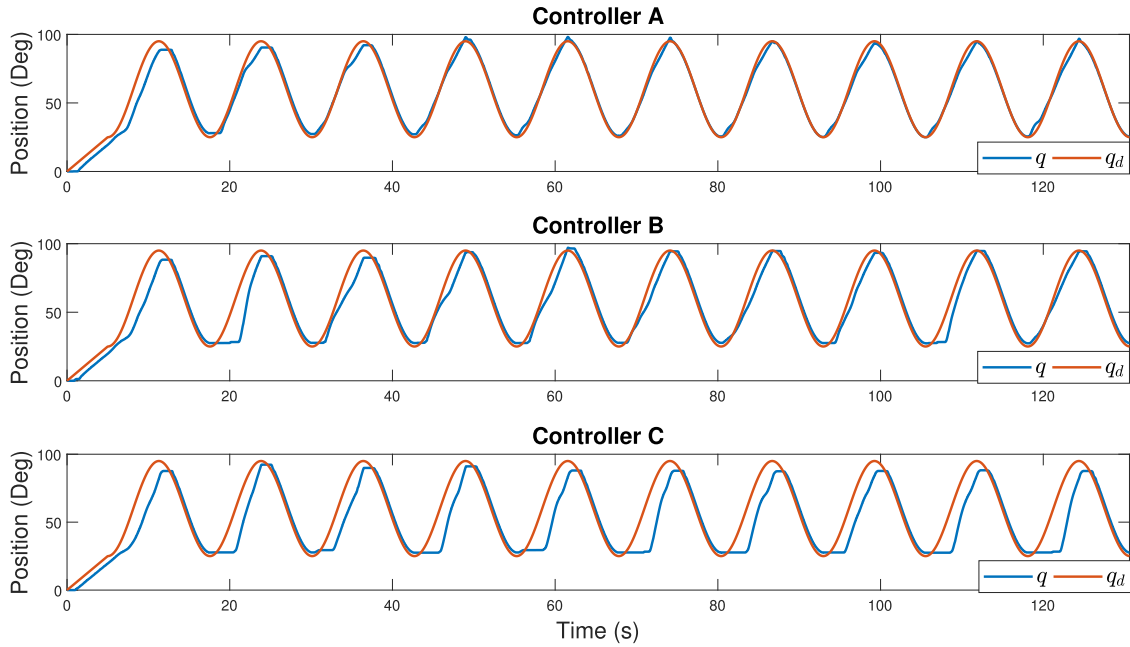


Fig. 2. The actual (q) versus the desired (q_d) position for each controller for a single participant.

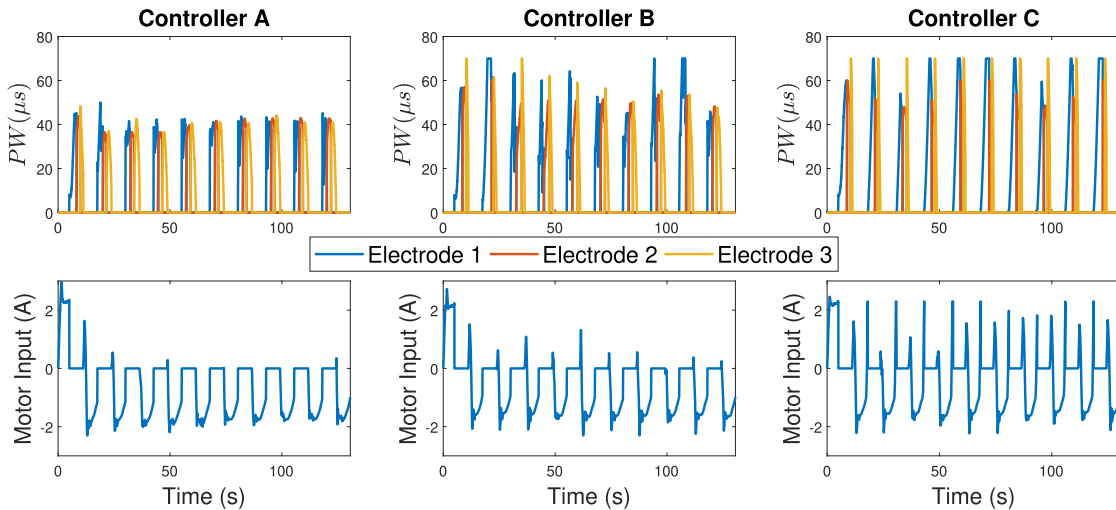


Fig. 3. The FES pulse width (PW) input applied to each electrode and the motor input for Controller A (left), Controller B (middle), and Controller C (right) for a single participant. A 0.5 s moving average filter was applied to the motor input for visual clarity.

relative to a traditional adaptive controller (Controller B). Furthermore, Controller A produced a significantly less variable FES control effort relative to both Controllers B and C, which may lead to a more comfortable experience for the participant. It should be noted that experiments were unable to be performed on participants with movement disorders due to Covid-19; however, the authors' have observed similar trends for participants with and without neurological conditions previously, although the tracking errors and control inputs tend to be larger for the former group [32], [33], [34]. Therefore, it is expected that Controller A would outperform Controllers B and C for participants with neurological conditions. Furthermore, the system identification performance is unable to be evaluated because the actual system parameters are unknown. However, visual inspection of Fig. 4 indicates

that different parameters were learned for Electrodes 1-3, which was expected due to each electrode likely having a different control effectiveness.

The effect of adaptation on position tracking can be investigated by comparing the results for each curl group in Table I. In fact, from Curls 1-3 to Curls 4-7, the RMS position error decreased by 46.8%, 29.0%, and 1.2% for Controllers A, B, and C, respectively, and the peak position error decreased by 40.8%, 33.4%, and 3.6% for Controllers A, B, and C, respectively. In fact, the statistical analysis confirmed that the median RMS and peak position errors decreased from Curls 1-3 to 4-7 and from Curls 1-3 to 8-10 for both Controllers A and B. Furthermore, from inspection of Table I the RMS and peak position errors changed minimally (|percent change| < 10%) from Curls 4-7 to 8-10 for each controller, which was

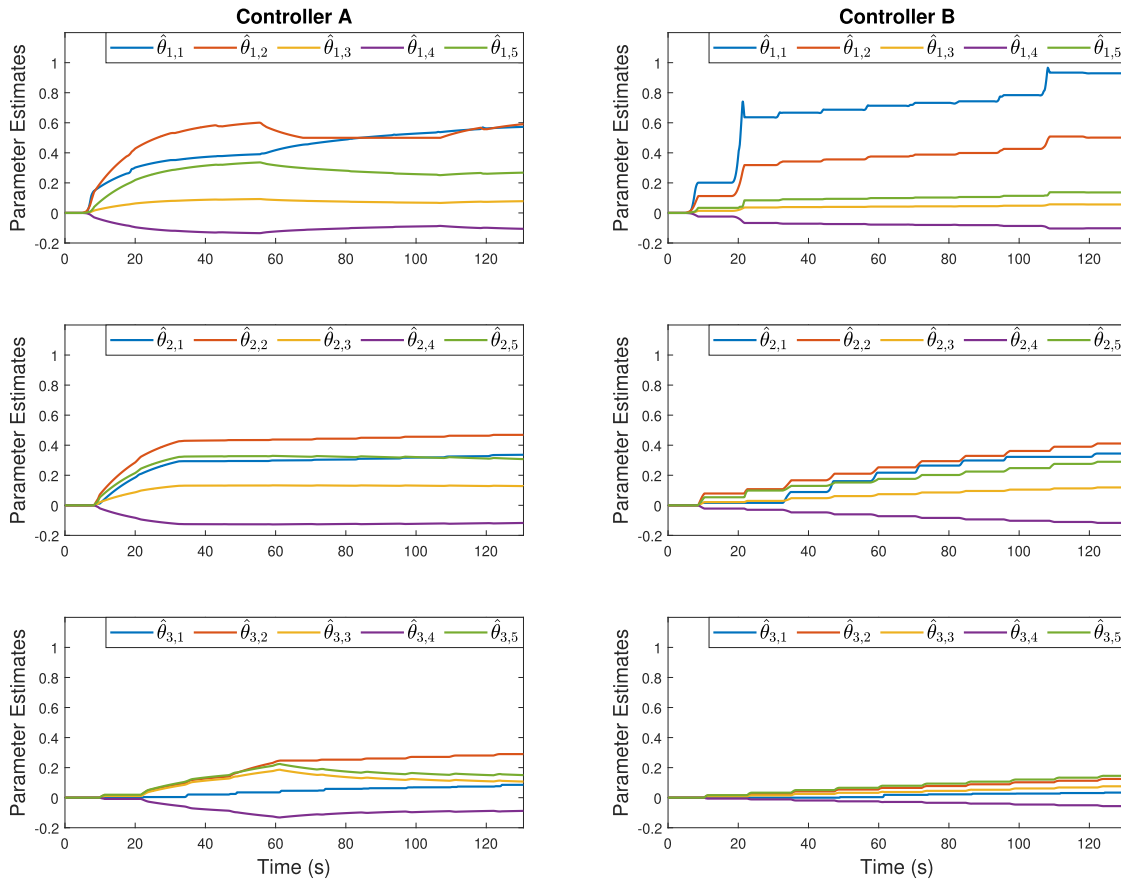


Fig. 4. The parameter estimates for Electrodes 1-3 for Controller A (left) and Controller B (right) for a single participant..

confirmed by the statistical analysis. Overall, the tracking performance was similar across curl groups for Controller C, which was expected since Controller C implemented a robust control law. However, both Controllers A and B implemented adaptive control terms, which resulted in the tracking performance improving from Curls 1-3 to Curls 4-7, as confirmed by the statistical analysis for Controllers A and B. Interestingly, there were minimal improvements from Curls 4-7 to Curls 8-10 for controllers A and B, which can be partly explained by inspection of Fig. 2. In Fig. 2, the position tracking tended to improve with each curl until Curl 8 for Controller A and Curl 9 for Controller B, at which point the performance slightly worsened and then began to improve again. In this work, the control effectiveness was assumed to be constant, but it is possible that fatigue caused the control effectiveness to decrease during the later curls, which required the parameter estimates to adjust accordingly as depicted in Fig. 4.

The effect of adaptation on the control inputs can likewise be investigated by comparing the results for each curl group in Table I. Overall, the motor effort had minimal changes across each curl group for each controller, which is confirmed visually in Fig. 3 and by the statistical analysis. Furthermore, as confirmed by the statistical analysis, the FES mean had negligible changes across each curl group for each controller and the SD of the FES effort had negligible changes across each curl group for Controllers B and C. However, for

Controller A, the SD of the FES effort decreased by 16.2% from Curls 1-3 to 4-7 and by 13.5% from Curls 4-7 to Curls 8-10, and the statistical analysis confirmed that the FES variance significantly decreased from Curls 1-3 to Curls 4-7 and from Curls 1-3 to Curls 8-10. Another important observation is that the position tracking improved significantly between Curls 1-3 and Curls 4-7 for Controller A, but the FES variation decreased and the median motor and FES efforts had negligible changes from Curls 1-3 and Curls 4-7. Therefore, the ICL-based adaptation was able to improve the tracking performance and decrease the FES variance without increasing the median control effort.

VIII. CONCLUSION

Adaptive ICL motor and FES controllers that use data-based and opportunistic learning were developed for a hybrid biceps curl exoskeleton. Global exponential trajectory tracking and parameter identification were guaranteed through a Lyapunov-like switched systems stability analysis. FES was allowed to switch between multiple electrodes on the biceps brachii and the motor effectiveness was uncertain, which required a unique set of parameters to be opportunistically learned for each subsystem. Experiments were performed on twelve healthy participants to compare the developed control system, a traditional adaptive controller, and a robust controller, which resulted in average position tracking errors of 0.28 ± 3.53 deg, 1.47 ± 5.78 deg, and

3.36 ± 7.97 deg, respectively, across a 10 curl experiment. A clinically significant feature of ICL is that the uncertain human and testbed parameters can potentially be identified in real-time. Future research will focus on extending the results to multiple degree-of-freedom testbeds, including experiments on participants with neurological conditions, and validating the parameter estimation performance and investigating if parameters can be learned more efficiently or accurately through intelligent modifications to the desired trajectory. Furthermore, the results indicated that fatigue may effect the performance of the controller during the later biceps curls. Therefore, future efforts will seek to incorporate fatigue in the dynamic model and to develop a means to compensate for its effects.

ACKNOWLEDGMENT

Any opinions, findings and conclusion, or recommendations expressed in this material are those of the author(s) and do not necessarily reflect the views of the sponsoring agency.

REFERENCES

- [1] C. Rouse, C. Cousin, V. H. Duenas, and W. E. Dixon, "Varying motor assistance during biceps curls induced via functional electrical stimulation," in *Proc. ASME Dyn. Syst. Control Conf.*, Nov. 2018, pp. 1–8.
- [2] C. A. Rouse, V. H. Duenas, C. Cousin, A. Parikh, and W. E. Dixon, "A switched systems approach based on changing muscle geometry of the biceps brachii during functional electrical stimulation," *IEEE Control Syst. Lett.*, vol. 2, no. 1, pp. 73–78, Jan. 2018.
- [3] C. A. Rouse, B. C. Allen, and W. E. Dixon, "Switched control of motor assistance and functional electrical stimulation for biceps curls," *Appl. Sci.*, vol. 22, no. 10, pp. 1–14, Nov. 2020.
- [4] E. J. Gonzalez, R. J. Downey, C. A. Rouse, and W. E. Dixon, "Influence of elbow flexion and stimulation site on neuromuscular electrical stimulation of the biceps brachii," *IEEE Trans. Neural Syst. Rehabil. Eng.*, vol. 26, no. 4, pp. 904–910, Apr. 2018.
- [5] E. S. Idsø, T. Johansen, and K. J. Hunt, "Finding the metabolically optimal stimulation pattern for FES-cycling," in *Proc. Conf. Int. Funct. Electr. Stimulation Soc.*, Bournemouth, U.K., Sep. 2004, pp. 1–3.
- [6] Z. Li, M. Hayashibe, C. Fattal, and D. Guiraud, "Muscle fatigue tracking with evoked EMG via recurrent neural network: Toward personalized neuroprosthetics," *IEEE Comput. Intell. Mag.*, vol. 9, no. 2, pp. 38–46, May 2014.
- [7] Z. Hussain, M. A. Zaidan, M. O. Tokhi, and R. Jailani, "The adaptive control of FES-assisted indoor rowing exercise," in *Proc. Int. Autom. Control Conf. (CACCS)*, Nov. 2009, pp. 1–6.
- [8] V. H. Duenas, C. A. Cousin, A. Parikh, P. Freeborn, E. J. Fox, and W. E. Dixon, "Motorized and functional electrical stimulation induced cycling via switched repetitive learning control," *IEEE Trans. Control Syst. Technol.*, vol. 27, no. 4, pp. 1468–1479, Jul. 2019.
- [9] V. Duenas, C. A. Cousin, V. Ghanbari, E. J. Fox, and W. E. Dixon, "Torque and cadence tracking in functional electrical stimulation induced cycling using passivity-based spatial repetitive learning control," *Automatica*, vol. 115, pp. 1–9, May 2020.
- [10] K.-M. Wang, T. Schauer, H. Nahrstaedt, and J. Raisch, "Iterative learning control of cadence for functional electrical stimulation induced cycling in Paraplegia," in *Proc. Conf. Int. Funct. Electr. Stimulation Soc.*, Sep. 2009, pp. 71–73.
- [11] V. H. Duenas, C. A. Cousin, C. Rouse, E. J. Fox, and W. E. Dixon, "Distributed repetitive learning control for cooperative cadence tracking in functional electrical stimulation cycling," *IEEE Trans. Cybern.*, vol. 50, no. 3, pp. 1084–1095, Mar. 2020.
- [12] C. A. Cousin, C. A. Rouse, and W. E. Dixon, "Split-crank functional electrical stimulation cycling: An adapting admitting rehabilitation robot," *IEEE Trans. Control Syst. Technol.*, vol. 29, no. 5, pp. 2153–2165, Sep. 2021.
- [13] N. A. Alibeji, N. A. Kirsch, and N. Sharma, "A muscle synergy-inspired adaptive control scheme for a hybrid walking neuroprosthesis," *Frontiers Bioeng. Biotechnol.*, vol. 3, no. 203, pp. 1–13, Dec. 2015.
- [14] N. Sharma, C. M. Gregory, M. Johnson, and W. E. Dixon, "Closed-loop neural network-based NMES control for human limb tracking," *IEEE Trans. Control Syst. Technol.*, vol. 20, no. 3, pp. 712–725, May 2012.
- [15] M. Ferrarin, F. Palazzo, R. Riener, and J. Quintern, "Model-based control of FES-induced single joint movements," *IEEE Trans. Neural Syst. Rehabil. Eng.*, vol. 9, no. 3, pp. 245–257, Sep. 2001.
- [16] R. J. Downey, T.-H. Cheng, M. J. Bellman, and W. E. Dixon, "Switched tracking control of the lower limb during asynchronous neuromuscular electrical stimulation: Theory and experiments," *IEEE Trans. Cybern.*, vol. 47, no. 5, pp. 1251–1262, May 2017.
- [17] I. Karafyllis, M. Malisoff, M. de Queiroz, M. Krstic, and R. Yang, "Predictor-based tracking for neuromuscular electrical stimulation," *Int. J. Robust Nonlinear Control*, vol. 25, no. 14, pp. 2391–2419, Sep. 2015.
- [18] J. Casas, C. H. Chang, and V. H. Duenas, "Motorized and functional electrical stimulation induced cycling via switched adaptive concurrent learning control," in *Proc. ASME Dyn. Syst. Control Conf.*, Oct. 2020, pp. 1–8.
- [19] B. C. Allen, K. Stubbs, and W. E. Dixon, "Adaptive trajectory tracking during motorized and FES-induced biceps curls via integral concurrent learning," in *Proc. ASME Dyn. Syst. Control Conf.*, Oct. 2020, pp. 1–9.
- [20] J.-J. E. Slotine and W. Li, "On the adaptive control of robot manipulators," *Int. J. Robot. Res.*, vol. 6, no. 3, pp. 49–59, 1987.
- [21] J.-J. E. Slotine and L. Weiping, "Adaptive manipulator control: A case study," *IEEE Trans. Autom. Control*, vol. AC-33, no. 11, pp. 995–1003, Nov. 1988.
- [22] B. D. O. Anderson, "Adaptive systems, lack of persistency of excitation and bursting phenomena," *Automatica*, vol. 21, no. 3, pp. 247–258, May 1985.
- [23] S. B. Roy, S. Bhasin, and I. N. Kar, "A UGES switched MRAC architecture using initial excitation," *IFAC-PapersOnLine*, vol. 50, no. 1, pp. 7044–7051, Jul. 2017.
- [24] S. K. Jha, S. B. Roy, and S. Bhasin, "Initial excitation-based iterative algorithm for approximate optimal control of completely unknown LTI systems," *IEEE Trans. Autom. Control*, vol. 64, no. 12, pp. 5230–5237, Dec. 2019.
- [25] G. V. Chowdhary and E. N. Johnson, "Theory and flight-test validation of a concurrent-learning adaptive controller," *J. Guid., Control, Dyn.*, vol. 34, no. 2, pp. 592–607, Mar. 2011.
- [26] G. Chowdhary, T. Yucelen, M. Mühlegg, and E. N. Johnson, "Concurrent learning adaptive control of linear systems with exponentially convergent bounds," *Int. J. Adapt. Control Signal Process.*, vol. 27, no. 4, pp. 280–301, Apr. 2013.
- [27] R. Kamalapurkar, B. Reish, G. Chowdhary, and W. E. Dixon, "Concurrent learning for parameter estimation using dynamic state-derivative estimators," *IEEE Trans. Autom. Control*, vol. 62, no. 7, pp. 3594–3601, Jul. 2017.
- [28] A. Parikh, R. Kamalapurkar, and W. E. Dixon, "Integral concurrent learning: Adaptive control with parameter convergence using finite excitation," *Int. J. Adapt. Control Signal Process.*, vol. 33, no. 12, pp. 1775–1787, Dec. 2019.
- [29] Z. I. Bell, J. Nezhadovitz, A. Parikh, E. M. Schwartz, and W. E. Dixon, "Global exponential tracking control for an autonomous surface vessel: An integral concurrent learning approach," *IEEE J. Ocean. Eng.*, vol. 45, no. 2, pp. 362–370, Apr. 2020.
- [30] A. F. Filippov, "Differential equations with discontinuous right-hand side," in *Fifteen Papers on Differential Equations* (American Mathematical Society Translation), vol. 42. Providence, RI, USA: American Mathematical Society, 1964, pp. 199–231.
- [31] N. Fischer, R. Kamalapurkar, and W. E. Dixon, "LaSalle-Yoshizawa corollaries for nonsmooth systems," *IEEE Trans. Autom. Control*, vol. 58, no. 9, pp. 2333–2338, Sep. 2013.
- [32] B. C. Allen, K. J. Stubbs, and W. E. Dixon, "Position and cadence tracking of a motorized FES-cycle with an unknown time-varying input delay using saturated FES control," *Automatica*, vol. 139, May 2022, Art. no. 110176.
- [33] B. C. Allen, C. A. Cousin, C. A. Rouse, and W. E. Dixon, "Robust cadence tracking for switched FES-cycling with an unknown time-varying input delay," *IEEE Trans. Control Syst. Technol.*, vol. 30, no. 2, pp. 827–834, Mar. 2022.
- [34] B. C. Allen, K. J. Stubbs, and W. E. Dixon, "Characterization of the time-varying nature of electromechanical delay during FES-cycling," *IEEE Trans. Neural Syst. Rehabil. Eng.*, vol. 28, no. 10, pp. 2236–2245, Oct. 2020.